Molecular Dynamics Simulations of Polyamide Membrane, Calcium Alginate Gel, and Their Interactions in Aqueous Solution

ARTICLE *in* LANGMUIR · JULY 2014

Impact Factor: 4.46 · DOI: 10.1021/la501811d · Source: PubMed

4 AUTHORS, INCLUDING:

Yuan Xiang
Chinese Academy of Sciences
5 PUBLICATIONS **19** CITATIONS
SEE PROFILE

Baoxia Mi
University of Maryland, College Park
14 PUBLICATIONS **262** CITATIONS
SEE PROFILE

Yongsheng Leng
George Washington University
56 PUBLICATIONS **767** CITATIONS
SEE PROFILE

Langmuir

Article

pubs.acs.org/Langmuir

Molecular Dynamics Simulations of Polyamide Membrane, Calcium Alginate Gel, and Their Interactions in Aqueous Solution

Yuan Xiang,[†] Yaolin Liu,[‡] Baoxia Mi,[‡] and Yongsheng Leng*[,†]

[†]Department of Mechanical & Aerospace Engineering, The George Washington University, Washington, D.C. 20052, United States
[‡]Department of Civil & Environmental Engineering, University of Maryland, College Park, Maryland 20742, United States

ABSTRACT: We perform molecular dynamics (MD) simulations to investigate the cross-linked polyamide (PA) membrane, the aggregation of alginate molecules in the presence of Ca^{2+} ions, and their molecular binding mechanism in aqueous solution. We use a steered molecular dynamics (SMD) approach to simulate the unbinding process between a PA membrane and an alginate gel complex. Simulation results show that Ca^{2+} ions are strongly associated with the carboxylate groups in alginate molecules, forming a web structure. The adhesion force between alginate gel and PA surface during unbinding originates from several important molecular interactions. These include the short-range hydrogen bonding and van der Waals attraction forces, and the ionic bridge binding that extends much longer pulling distances due to the significant chain deformations of alginate gel and PA membrane.

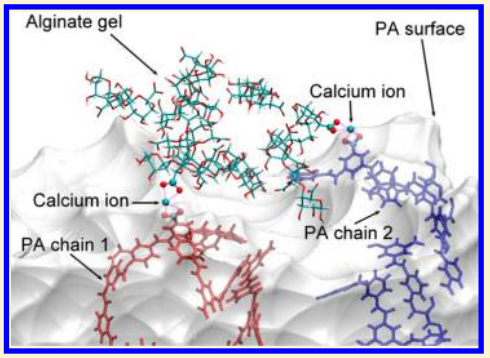

1. INTRODUCTION

The shortage of portable water is a globally challenging problem in our future.[1,2] Membrane separation, since its development in the 1960s, is considered to be a very promising technique to address this issue. In recent years, several methods based on semipermeable membrane processes, including reverse osmosis (RO), nanofiltration (NF), and emerging forward osmosis (FO), evolved rapidly for drinking water purification.[3−5] However, membrane techniques also have their own shortcomings. One of the important issues is membrane fouling, which could significantly reduce membrane performance, such as water flux and effluent quality.[6,7]

To understand the underlying mechanisms of membrane fouling, molecular simulations provide a powerful tool to elucidate the molecular origin and new fundamental insights into this fouling, and may change our way of thinking about the membrane fouling phenomenon. In general, two types of molecular interactions, the foulant−foulant and foulant−membrane interactions, and their competitions with each other, can dramatically influence membrane fouling. Recent simulation studies on the foulant−foulant interactions[8−11] revealed several binding mechanisms. Kalinichev et al. reported the binding behavior of Ca^{2+} metal ions with natural organic matter (NOM) in aqueous solutions.[9] They found that Ca^{2+} ions have strong binding with carboxylic groups in NOM and indicated that this could be a driving force for the NOM aggregation.[9] Plazinski and Rudzinski studied gelling of alginates in the presence of divalent metal ions.[12] They concluded that the association of alginate chains is mediated by calcium ions and carboxylic groups that form stable configurations. For the foulant−membrane interactions, very few molecular simulations have been reported. Ahn et al. probed the interactions between a NOM molecule and a poly(ether sulfone) (PES) membrane.[13] They focused on the association of different metal ions with PES membrane and NOM surfaces. However, the real interactions between NOM and membrane surfaces were not directly addressed in their study.

In our recent simulation work, we reported single alginate molecule and its interaction with polyamide (PA) membrane surface.[14] PA is selected as a model semipermeable membrane because it is the most widely used RO membrane material and has been studied extensively by other researchers,[15−21] while alginate is widely distributed in the environment and is believed to be one of the major contributors to organic fouling.[22−24] Through a steered molecular dynamics (SMD) simulation, we demonstrated that metal ions can form very strong ionic binding complexes between the alginate molecule and PA surface through "ionic bridge". We further analyzed different binding structures and their binding strengths in different alginate−ion−membrane systems.

In the present study, we investigate the fouling mechanism when a multialginate gel is in contact with a PA surface in the presence of calcium ions. This situation is more general and realistic, though more complicated than those of single alginate−PA interactions. Our focus will be on the origin of gel−membrane binding forces. More explicitly, besides the ionic bridging forces, we will look into other major forces and factors that could contribute to membrane fouling. The effect of different metal ions on the formation of alginate gels will also be investigated. In section 2, we briefly describe the methodology of building amorphous PA membrane model.

Received: May 11, 2014
Revised: July 7, 2014
Published: July 14, 2014

dx.doi.org/10.1021/la501811d | *Langmuir* 2014, 30, 9098−9106

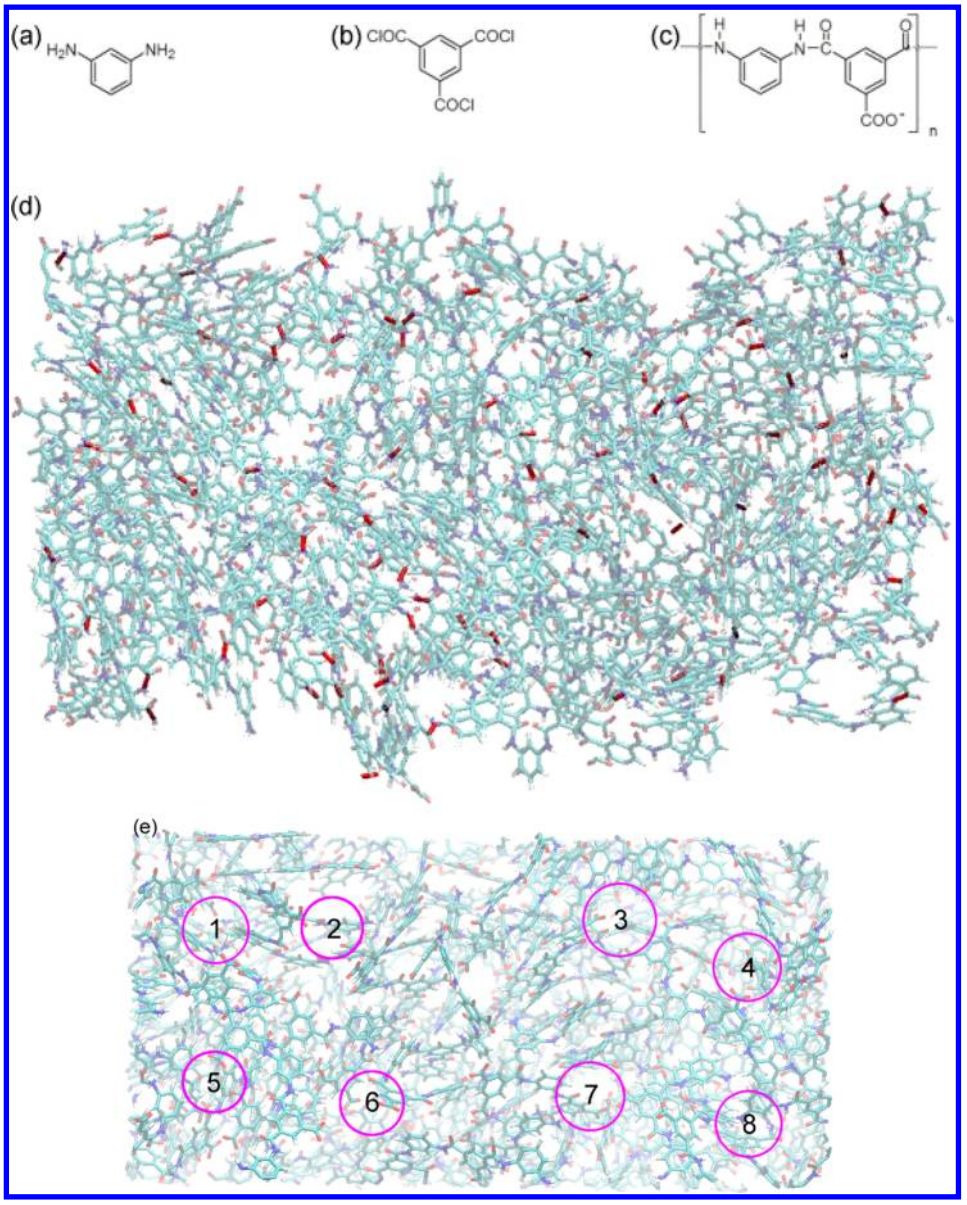

Figure 1. (a) Meta-phenylenediamine (MPD) molecule. (b) Benzene-1,3,5-tricarboxylic acid chloride (TMC) molecule. (c) Repeat unit in the polyamide chain molecule. (d) Snapshot of cross-linking PA membrane. The new cross-linking C−N bonds between PA chains are highlighted as red lines. (e) Top view of the equilibrated PA membrane surface in water. The purple circles indicate the locations where the SMD unbinding simulations are performed. Color code: red, O; white, H; light blue, C; dark blue, N.

Simulation results will be discussed in section 3, followed by our summary in section 4.

2. MOLECULAR MODELS AND SIMULATION METHODS

2.1. Molecular Models. *2.1.1. PA Membrane.* PA membrane is made from the polymerization of meta-phenylenediamine (MPD, Figure 1a) and benzene-1,3,5-tricarboxylic acid chloride (TMC, Figure 1b) monomers. The protocol of building polyamide membrane is similar to our previous publication.[14] Generally, three main steps are performed. The *first* step is to fold the linear PA chains into the simulation box based on the configurational-bias Monte Carlo algorithm.[25] This algorithm could significantly increase the acceptance rate for insertions of polyatomic chain molecules and in the meantime allow for all chain conformations generated with the correct Boltzmann weight.[26] A total of 18 PA chain molecules are folded into the simulation box with each chain molecule containing 12 repeated units (Figure 1c).

The *second* step is to create cross-linking structure for both intra- and intermolecular chains. We use a common protocol first proposed by Kotelyanskii et al.[18,19] and now adopted by several other research groups.[16,17,27] MPD monomers are randomly inserted into the initially non-cross-linked PA membrane. After several energy minimizations, MPD monomers are allowed to be connected with the carboxylate groups in PA chains to form cross-linking structures. The rule of building these structures is based on the distance between the carboxylate carbon atom in PA membrane and the amine nitrogen atom in MPD. If the two amine nitrogen atoms in one MPD are within 6.5 Å distance of the corresponding carboxylate carbon atoms in the PA membrane, then the two new C−N bonds will be created to form a cross-linking in the PA membrane. At the same time, one oxygen atom in each of the original carboxylate groups in the PA membrane and one hydrogen atom in each of the original amine groups in MPD will be removed. MPD monomers that do not fully participate in cross-linking will be eventually deleted. One of the advantages of this protocol is that we can directly control the cross-linking rate by inserting a predetermined number of MPD monomers. We can take

dx.doi.org/10.1021/la501811d | *Langmuir* 2014, 30, 9098−9106

this quantity as an adjustable parameter to fit experimental data. The final configuration of PA membrane is shown in Figure 1d with a cross-linking rate at about 60%, which approximately matches the experimental result.[28−31]

The *third* step is to introduce water molecules into the simulation system to fully hydrate the cross-linked PA membrane. For the current simulation system, we introduce a total of 6560 water molecules to hydrate the amorphous PA membrane, whose dimensions are around 72 Å × 36 Å × 40 Å. A total of 96 sodium ions are also added to the system to balance the charged sites in PA membrane. A vapor phase is maintained above the water−PA complex, allowing the system pressure to be comparable to the water vapor pressure.[32,33] After an equilibrium molecular dynamics (MD) run of over 10 ns, the density of the hydrated PA membrane is found to be around 1.35 g/cm^3 (the density of PA membrane itself after subtracting water content is about 1.1 g/cm^3). The result is consistent with experimental (1.38 g/cm^3) and other simulation results.[16,17,19]

2.1.2. Alginate Foulant. Alginates are linear polymer chains containing β-D-(1→4)-mannuronic acid (M) and α-L-(1→4)-guluronic acid (G) residues. In this study, we focus on the polymeric chains that only consists of α-L-(1→4)-guluronic acid (G) residues. This selection is based on their specific spacing and geometry of the carboxylate functional groups for cation binding.[34] The strong interactions between the divalent ions and G residues lead to the association of chains to form alginate gel, which is believed to be one of the main contributors to organic fouling.[12] Figure 2 shows the

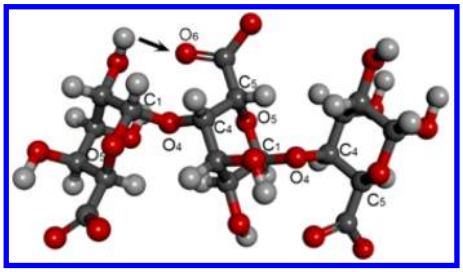

Figure 2. Structure of the alginate molecule that contains three L-guluronic acid (G) residues. Color code: red, O; white, H; and gray, C. The arrow indicates one possible hydrogen bond.

molecular model of alginate consisting of three L-guluronic acid (3G) residues. According to the acid dissociation constant (pK_a) of alginic acid (3.38−3.65),[35,36] under the neutral pH condition all the carboxyl groups should be deprotonated.[36] Therefore, we introduce three sodium ions (Na^+) for each alginate molecule to compensate the negatively charged sites on deprotonated carboxyl groups. A total of 27 Na^+ cations are added to the simulation system for the 9 alginates.

To investigate the effect of different metal ions on the formation of alginate gels, Ca^{2+} ions are also introduced into the simulation system. Details of the simulation procedure will be further discussed in section 3.1. The conformation of the alginate chain is mainly determined by two torsional angles (see Figure 2): Φ ($O_5-C_1-O_4-C_4$) and Ψ ($C_1-O_4-C_4-C_5$). According to previous studies,[34] a common global energy minimum for the disaccharide models is at $\Phi = 274° \pm 7°$ and $\Psi = 227° \pm 5°$. The initial torsional angles of Φ and Ψ in alginate chains are set based on the above data.

2.2. Force Field and Simulation Method. The detailed MD simulation procedures are similar to those described in our previous work.[14] We use LAMMPS computational package for all of the MD simulations.[37] Periodic boundary conditions are applied in the three directions. We use consistent valence force field (CVFF)[38] to describe the interactions of alginate molecules and the PA membrane. This force field has been parametrized for organic molecules containing aromatic, amine, amide, hydroxyl, and carboxylate groups and, therefore, is well-suited for our system. We employ the flexible simple point charge (SPC) water model[39,40] which is compatible with the CVFF. For the ion−water interactions we use Aqvist's SPC water compatible potentials[41] for the monovalent Na^+ and divalent Ca^{2+} ions. As Aqvist's parameters are only available for alkali and alkaline-earth metal cations, we choose the potential parameters for halide Cl^- ion calculated by Joung and Cheatham.[42] The particle-particle-particle-mesh solver is used to calculate long-range electrostatic interactions.[43] The cutoff distance for the short-range Lennard−Jones interactions is set to 10 Å. The equations of motion of particles are propagated via the velocity Verlet algorithm with a time step of 1 fs in constant-NVT ensemble. The temperature is controlled at 300 K using the Nose-Hoover thermostat. We also use the NPT MD simulations to investigate the formation and configuration of alginate gel and the ion exchange phenomenon. The temperature and pressure of these simulations are controlled at 300 K and 1 bar, respectively. The steered molecular dynamics (SMD) simulation is performed to calibrate the binding strength of the gel−membrane system. The center of mass (COM) of the alginate gel is connected to a driving spring to mimic the adhesion force measurement in experiments. The variation of the quasistatic spring force versus pulling distance will give a force−distance profile for the binding site. The detailed SMD simulation method is described in our previous work.[14]

3. RESULTS

3.1. Aggregation of Multiple Alginates and Gel Formation. The interactions between ions and foulants have been investigated by many research groups.[8,10,12,34,44−48] It has been reported that Ca^{2+} ion can significantly promote the aggregation of alginate chains.[10,12,47,48] Previous simulation studies usually focused on alginate aggregation in pure water. In our present study, we investigate the aggregation behavior of alginates in different ion environments. Here, the monovalent sodium ions and divalent calcium ions may coexist, leading to possible competition in ion binding and ion exchange during the gel formation. Two independent NPT MD simulations are performed at T = 300 K and P = 1 bar pressure. In the first simulation, the system contains 9 3G alginate molecules and 3504 water molecules, together with 27 Na^+ ions to balance the charged sites in carboxylate groups. In the second simulation, the system contains an *extra* 18 Ca^{2+} ions and 36 Cl^- co-ions, corresponding to a $CaCl_2$ solution with a concentration of 0.25 M. Initially, all of the Na^+ ions are intentionally placed close to the negatively charged carboxylate groups, and the Ca^{2+} and Cl^- ions are distributed randomly in the solution. The initial distance of Na^+-O (in $-COO^-$) is about 0.21−0.24 nm, corresponding to the local energy minimum of the system.[14,49] During the MD simulation, we are able to observe how Ca^{2+} ions can exchange Na^+ ions, leading to gel formation.

To quantify the degree of alginate aggregation, we adopt a similar approach proposed by Kalinichev et al.[9] The center of mass (COM) of each alginate molecule is monitored throughout the simulation, and the radial distribution function (RDF) of COM is calculated at different time period. For the 20 ns MD simulation run, we divide the whole process into 20 segments at 1 ns intervals and monitor the evolution of the RDF versus time. Figure 3 shows the RDFs at the 10th and 20th nanosecond for system 1 (with only Na^+ existing) and system 2 (with Na^+, Ca^{2+}, and Cl^- coexisting). For system 2, the peak at around 7 Å is quite obvious, indicating the very strong, Ca^{2+}-induced aggregation of alginate molecules and the ion exchange process of Na^+ by Ca^{2+}. The degree of this aggregation could also be seen by looking at the different RDF curves at the 10th and 20th nanosecond time period (Figure 3). In contrast, system 1 with only Na^+ present does not show strong evidence of alginate aggregation. The RDF curve at the 20th nanosecond exhibits more random, nonaggregated structure.

dx.doi.org/10.1021/la501811d | *Langmuir* 2014, 30, 9098−9106

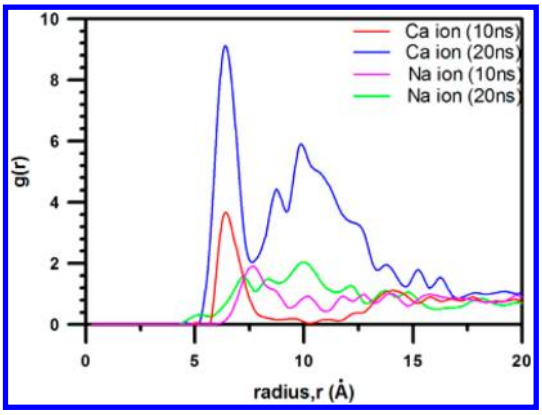

Figure 3. Time evolution of radial distribution functions (RDF) of the center of mass (COM) of alginate molecules in different ion systems during equilibrium simulation runs.

To further give insights into the structure of alginate gels in Ca^{2+} ions solution, we calculate the coordination numbers of oxygen around the hydrated metal ions Ca^{2+} and Na^{+}. Figure 4 shows the detailed partition of oxygen atoms from different species. The figure clearly shows that the total coordination numbers for Ca^{2+} and Na^{+} in the first hydration shell are about eight and six, respectively. From the calculation, we find that the major contribution to the coordination comes from the carboxylate group in alginate and water molecules in the first hydration shell. Other negatively charged oxygen species, such as the oxygen atoms from the hydroxyl or ether groups of alginate, contribute much less (less than 0.5) to the total coordination number. Note that the coordination number for Na^{+}−O (carboxylate) pair is almost zero (Figure 4b), indicating that Na^{+} ions are completely exchanged by Ca^{2+} ions. Further calculations show that, out of 18 Ca^{2+} ions, there are 10−11 Ca^{2+} ions with each of them coordinated by four carboxyl oxygens from two opposite carboxylate groups belonging to two different chains (the so-called two-bidentate configuration;[9] see Figures 4a and 5) and, additionally, by four oxygens from water molecules. Further, there are other four to five Ca^{2+} ions with each of them coordinated by two oxygens from one carboxylate group (the so-called bidentate configuration[9]) and six oxygens from water molecules. The remaining Ca^{2+} ions are fully hydrated in aqueous solution. These results for the coordinate numbers of Ca^{2+} and Na^{+} ions are consistent with other simulation studies.[50,51]

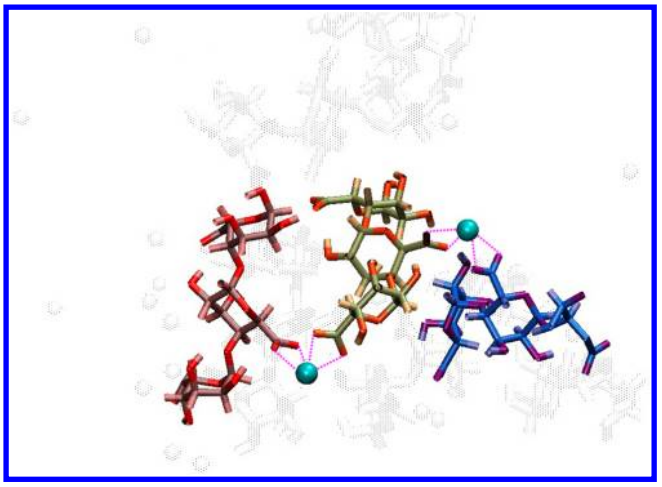

Figure 5. Two-bidentate binding structures of Ca^{2+} alginate gel. Each of the two coordinated Ca^{2+} ions are connected to two carboxylate groups from the two different alginate chains. The Ca^{2+}−O bindings are shown by the purple lines. Ca^{2+} ions are represented in cyan.

Figure 5 shows one of the typical equilibrium structures of calcium alginate gel. Here we only display three alginate chains and the coordinated Ca^{2+} ions. The remaining alginate chains and ions are shown as transparent for clarity. The three different chains are tagged by different colors. It is seen that all of the alginate molecules are connected through calcium ions, forming a web structure. Each Ca^{2+} ion is associated with two carboxylate groups from two different alginate molecules, forming a two-bidentate binding state. The distances between Ca^{2+} ion and the coordinated oxygens are approximately equal to the same value of 2.4 Å.[41] In previous work, Plazinski and Rudzinski reported several possible stable alginate aggregation configurations.[12] The majority of them are formed by two or more carboxylate groups coordinating to Ca^{2+} ions in the first hydration shell. The present study shows that each Ca^{2+} ion tends to connect with only two carboxylate groups from two alginate molecules (corresponding to 1c configuration reported by Plazinski and Rudzinski[12]) and binding of Ca^{2+} ion with more than two carboxylate groups is not observed. Moreover, a few Ca^{2+} ions (less than 10% of total calcium ions) are coordinated by only one carboxylate oxygen (the so-called monodentate configuration[9]). We attribute this to the relatively high concentration of Ca^{2+} ions that provide sufficient binding cations for the two-bidentate or less populated monodentate

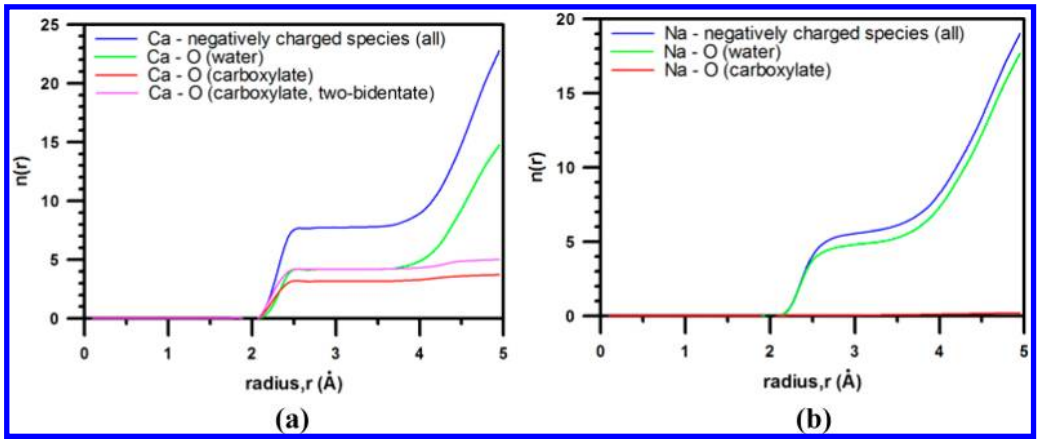

Figure 4. Coordination numbers around (a) Ca^{2+} ions and (b) Na^{+} ions in alginate−$CaCl_2$ solution.

dx.doi.org/10.1021/la501811d | *Langmuir* 2014, 30, 9098−9106

binding configurations. This alginate gel will be used in the subsequent gel−PA membrane interaction studies.

3.2. Interaction between Alginate Gel and PA Membrane: The Origin of Binding Forces and Associated Binding Structures. *3.2.1. Steered-MD Simulation and Binding Force Characteristics.* Upon the formation of Ca^{2+} alginate gel in $CaCl_2$ solution, the whole aqueous system is combined into the hydrated PA membrane to form a larger molecular simulation system, whose dimension is now increased to 72 Å × 36 Å × 130 Å. A very large vapor phase with a height of 400 Å in the normal direction is maintained above the aqueous liquid block. Figure 6 shows the molecular

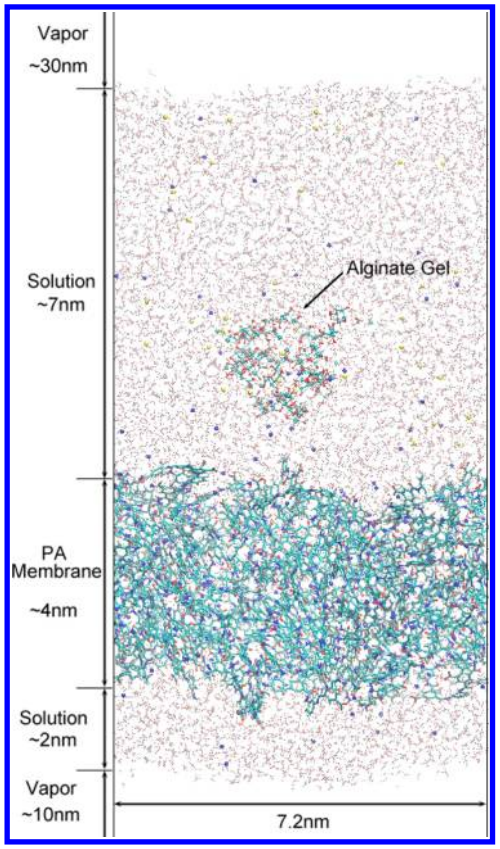

Figure 6. Molecular configuration of the simulation system, which includes the hydrated PA membrane, alginate gel and ions. Color code: red, O; white, H; light blue, C; dark blue, N. In solution: dark blue balls, Na^+ ions; light blue balls, Ca^{2+} ions; yellow balls, Cl^- co-ions.

configuration of the simulation system. The initial distance between the center of mass (COM) of alginate gel and the PA surface is about 2.5 nm. Following the same procedure used in our previous study,[14] a small pulling force in the range of 0.1−0.3 nN, which could be considered as a hydrodynamic force, is applied to drag the gel toward the PA surface. When the distance between the nearest gel−PA atom pair is within 0.5 nm, the pulling force is released and the alginate gel will dock onto the PA surface. We use this drag-and-release approach at eight different locations on the PA surface (Figure 1e). After an equilibrium time of over 10 ns, the steered molecular dynamics (SMD) simulation is performed to calibrate the binding strength of the gel−membrane system on each site. The detailed SMD simulation method is described in our previous work.[14] Basically, the COM of alginate gel is attached to a driving spring to mimic the adhesion force measurement in experiment. This COM is updated during SMD simulation to reflect the flexible changing of the gel geometry under pulling. The variation of the quasistatic spring force versus moving distance will give a force−distance profile for the specific binding site. The pulling speed is 0.015 Å/ps, a reasonable value in MD regime.

A typical averaged spring force curve is shown by the blue line in Figure 7. The force−distance variation exhibits an initial

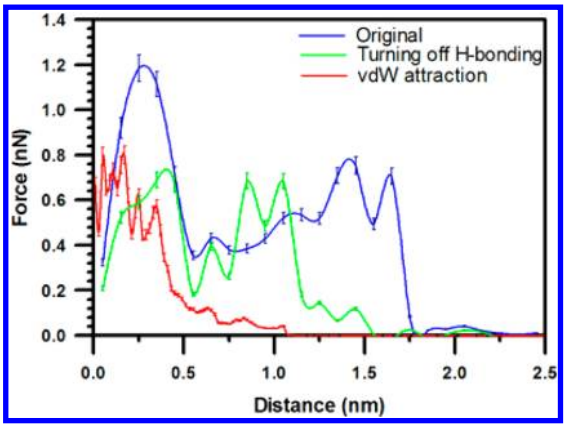

Figure 7. Averaged force−distance curves obtained from the SMD simulations for three situations. The blue line shows the original SMD force curve that includes all of the atomic interactions. The green line shows the force curve obtained by turning off H-bonding interaction (between oxygen atoms of carboxylate group in PA and the hydrogen atoms of hydroxyl group in alginate). The red line shows the van der Waals attraction force curve between the alginate gel and PA membrane.

large force peak, followed by two or more smaller force peaks until the final breakdown. These force peaks signify different molecular binding events and will be discussed in detail below. They also quantitatively reflect the adhesion forces at different binding stages and therefore may find practical applications in experimental measurements.

A total of eight SMD simulations at different locations on the PA membrane surface are performed. These binding sites on the PA surface are shown in Figure 1e. We find that although the distances at which the spring forces begin to increase dramatically are different at different locations, the characteristics of the force−distance curves are very similar and the force maxima at different locations are also comparable. In Figure 7, the blue line shows the averaged spring force-distance curve at the binding site 7 (Figure 1e) on the PA surface. There are essentially two binding stages during the gel−PA detachment: (1) The first force peak occurs at a distance between 0 and 5 Å with a value around 1−1.2 nN. This force peak is usually the global maximum during the breakdown, which is very different from the single alginate−PA membrane interactions.[14] We will show that this binding force is largely related to the hydrogen bonding (H-bonding) and van der Waals attraction forces between the alginate gel and PA membrane. (2) At the distance between 5 and 20 Å, there are one to two significant force peaks with a magnitude around 0.6−0.8 nN. Occasionally, there are more than two force peaks which count less than 10%. We will show that these force peaks are related to the ionic bridge binding, as has been seen in our previous study of single alginate−PA membrane interactions.[14]

dx.doi.org/10.1021/la501811d | *Langmuir* 2014, 30, 9098−9106

3.2.2. Deformation of Alginate Gel. An interesting question concerns how the alginate gel evolves in structure during the unbinding from PA surface. Unlike other high molecular weight foulants, such as NOM or small bacteria, the alginate gel is composed of individual molecular chains aggregated through cation-induced binding. Its packing structure may not be as compact as other foulants. Because of this binding character, the alginate gel should be more flexible to change its size and geometry. This property may have some consequence. For example, the gel may tend to adapt to the morphology of the membrane surface, increasing the contact area with PA membrane. Consequently, the size and geometry of the gel close to the membrane surface will be different from that in bulk water. To investigate the structural evolution of the gel during the unbinding process, we calculate the RDF of alginates in the gel at different pulling distances. Figure 8 shows the RDF

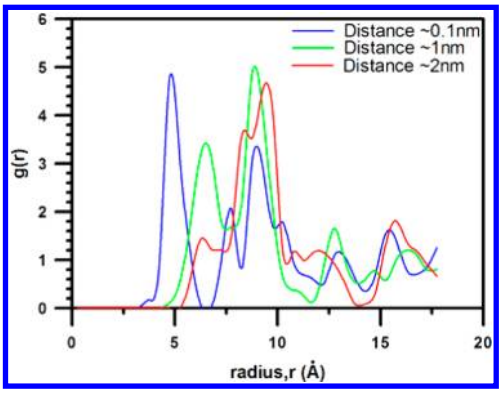

Figure 8. Radial distribution functions (RDFs) of the center of mass (COM) of alginate molecules at different pulling distance during the SMD simulation.

curves at three pulling distances. These RDFs are calculated based on the COM coordinates of alginate chains. When the gel is still in close contact with the PA membrane (the initial pulling distance of 0.1 nm), the first RDF peak is at 5 Å, which is at a much smaller distance than that in the bulk solution (7 Å; see Figure 3). This indicates that the packing of the gel is very compact due to strong attraction between the gel and PA membrane. As the alginate gel is gradually pulled off from the PA surface, the first RDF peak gradually shifts toward larger distances, indicating that the gel is becoming less compact. The implication of this "distance-dependent" volume change of the alginate gel near the PA membrane is that, in practical industry, the cross-flow cleaning technique[52] for PA membranes may not work well for alginate foulant, if the alginate gel is already attached to the PA surface.

3.2.3. Hydrogen Bonding and van der Waals Interactions. In Figure 7, the first large force peak occurring within 5 Å pulling distance indicates that there is a very strong, short-range interaction force existing between the alginate gel and PA membrane. Two possible short-range interactions may contribute to this strong binding force: the electrostatic and van der Waals interactions. It has been reported that the intramolecular hydrogen bonding (H-bonding) could happen within an alginate molecule consisting of G residues.[12] This is shown in Figure 2 where the favorable geometry of GG structure allows the H-bonding between the carboxylate O6 and the hydroxyl group in the contiguous monomer to be formed (indicated by the arrow in Figure 2). It is therefore instructive to find out whether the H-bonding between the alginate gel and the PA membrane could be formed when they are in close proximity. Based on the RDFs for different atomic pairs and the geometric criteria for H-bonding,[53] we find that the most possible contact pair for H-bonding comes from the carboxylate oxygen from the membrane surface and the hydroxyl hydrogen from the alginate molecule. In Figure 9,

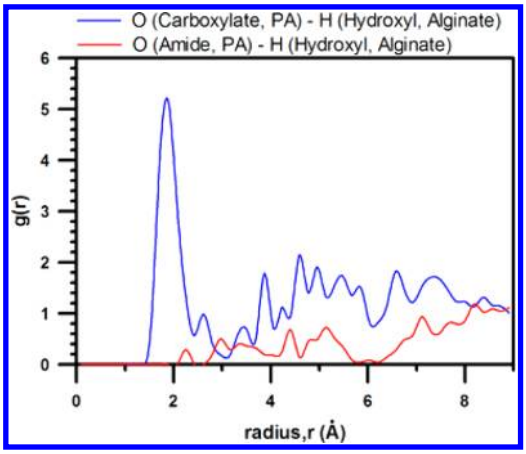

Figure 9. Radial distribution functions (RDFs) for the contact pairs between carboxylate oxygen in PA and the hydroxyl hydrogen in alginate (blue), and the contact pairs between the amide oxygen in PA and the hydroxyl hydrogen in alginate. The former RDF indicates the formation of strong H-bonding.

the blue line shows the RDF of the O (PA carboxylate)−H (alginate hydroxyl) contact pair. The first RDF peak at 2 Å distance signifies the formation of H-bonding. As a comparison, the RDF curve for the O (PA amide)−H (alginate hydroxyl) pair does not show any significant peak within short distances; in other words, no H-bonding is formed in between.

To further prove that the H-bonding has a major contribution to the first force peak in Figure 7, we deliberately turn off the O (carboxylate, PA)−H (hydroxyl, alginate) interactions (including electrostatic and van der Waals interactions). The new SMD force−distance curve is shown in Figure 7 by the green line. Evidently, the amplitude of the first force peak is decreased dramatically. Additionally, since the H-bonding directly influences the local hydration structure, artificially removing H-bonding also leads to the overall changes of the force−distance profile. For example, the last two force peaks in the original force curve are shifted to the left by roughly 5 Å. However, the magnitudes of these two force peaks have almost no change, suggesting that they come from different molecular interactions, which will be discussed in the next subsection.

In Figure 7 we also draw the force−distance curve due to the van der Waals (vdW) attraction (the r^{-6} term in LJ potential; see the red line) between the alginate gel and PA membrane, along the original pulling trajectory (the blue line). The vdW force clearly exhibits a fast decay within a distance of 5 Å, which accounts for almost 50% of the total binding force. Note that as this force curve is calculated based on the gel−PA membrane configurations along the SMD pulling trajectory; other effects such as hydrophobic attraction[54] between low charged species in PA and alginate molecules may contribute to the first large force peak. However, we believe that this should be the secondary effect. Our major conclusion is that the origin of the first large force peak shown in Figure 7 comes from the H-

dx.doi.org/10.1021/la501811d | *Langmuir* 2014, 30, 9098−9106

bonding and van der Waals interactions between the alginate gel and PA membrane.

3.2.4. Ionic Bridge Binding. The force peaks at distances between 5 and 20 Å, as shown in Figure 7, are mainly contributed from the ionic bridge bindings between the alginate gel and PA membrane. This could be easily verified by turning off the interactions between the carboxylate groups (including C and O atoms) in the PA membrane and the bridging Ca^{2+} ions. As shown in Figure 10, the new force curve (the red line)

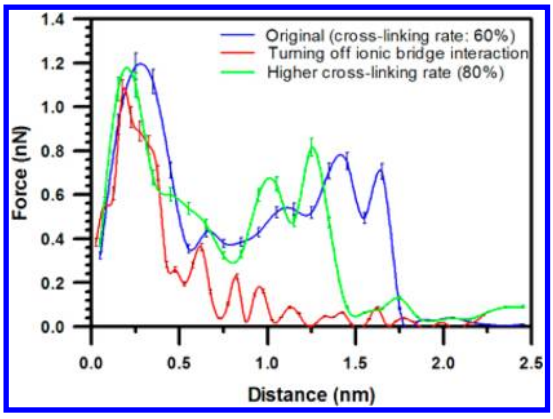

Figure 10. Averaged force–distance curves obtained from the SMD simulations for three situations. The blue line shows the original SMD force curve that includes all of the atomic interactions (the same as in Figure 7). The green line shows the new force curve when the cross-linking rate of the PA membrane reaches 80%. The red line shows the force curve obtained by turning off the pair interactions between the carboxylate groups in PA membrane and the calcium bridging ions.

does not show any significant force peaks at larger distances, while the first force peak contributed from the H-bonding and vdW interactions is almost intact. We emphasize that the artificial force curves, derived by turning off some force components as shown in Figures 7 and 10, do not represent any realistic physical processes. They are used solely for the purpose of identifying the different origins of binding forces.[55]

Figure 11 shows the two ionic binding configurations between the alginate gel and PA surface at the last two force peaks. Figure 11a shows that there are two Ca^{2+} ions forming two-bidentate, inner-sphere binding complexes at different binding sites. This binding configuration corresponds to the first ionic binding force peak in Figure 7 or 10. As the alginate gel is further pulled apart from the PA surface, one of the Ca^{2+} ionic bridges breaks down. Further pulling makes the ionic binding force approaches the last force peak in Figure 10, corresponding to the second snapshot in Figure 11b. It is often seen that ionic bridges are broken down subsequently during SMD simulations. Only in one case out of eight SMD runs did we observe the simultaneous breakdown of two ionic bridges.

From Figures 7 and 10, the H-bonding and vdW interactions are mainly responsible for the short-range adhesion forces (within 5 Å distance), while the ionic bridge binding interactions extend to a much longer distance due to the gel–PA deformation under pulling. These characteristics could also be observed by tracing the atomic pair distances during the unbinding process. Figure 12 shows a typical example in a SMD simulation. It is seen that the H-bonding pair breaks down within a pulling distance less than 2 Å, while the breakdown of the ionic bridge occurs at a pulling distance of 14 Å. A slightly larger pair distance of 3.8 Å before breakdown corresponds to

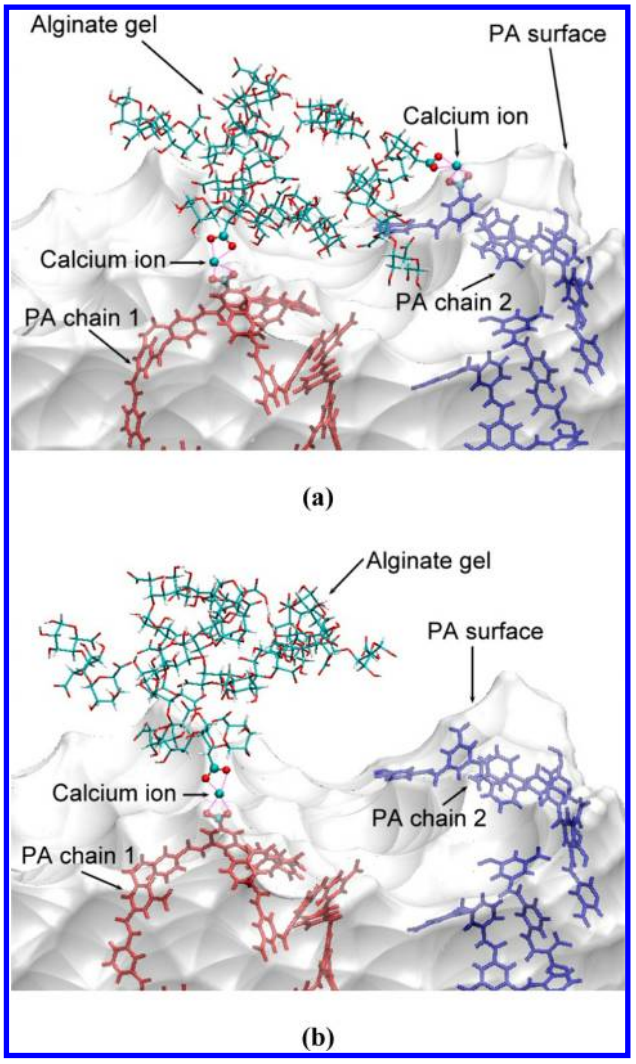

Figure 11. Snapshots of the alginate gel–membrane ionic binding during the SMD pulling. Configurations (a) and (b) correspond to the ionic binding force peaks at the pulling distances of 1.37 and 1.7 nm (see Figure 7), respectively. The ionic bridges are indicated by the purple lines. The two PA chains involved in the ionic bridges are distinguished by different colors. Other PA chains on the surface are represented by white surface for clarity. Water molecules and other ions are removed for clarity.

the monodentate configuration of Ca^{2+} ionic bridge. Obviously, the "survival pulling distance" for the ionic bridge binding is much longer than that of H-bonding. This phenomenon is clearly related to the short-range characteristics of H-bonding and the tenacious specific binding in ionic bridges.

However, it is anticipated that the degree of cross-linking, a measure of the rigidity of the PA membrane may influence the survival pulling distance of ionic bridges. To test this idea, we rebuild a membrane block with a higher cross-linking rate (about 80%, compared with the original 60%). The averaged force–distance curve is shown in Figure 10. The new force curve (green line) shows that the first H-bonding and vdW force peak, as well as the subsequent two ionic binding force peaks, have been shifted to smaller distances. In particular, the ionic force peaks move to the left by almost 5 Å. As shown in Figure 13, due to the near-surface cross-linking, the PA surface chain that connects to the alginate gel through calcium ion will not be able to move to a larger distance. Higher cross-linking

dx.doi.org/10.1021/la501811d | *Langmuir* 2014, 30, 9098–9106

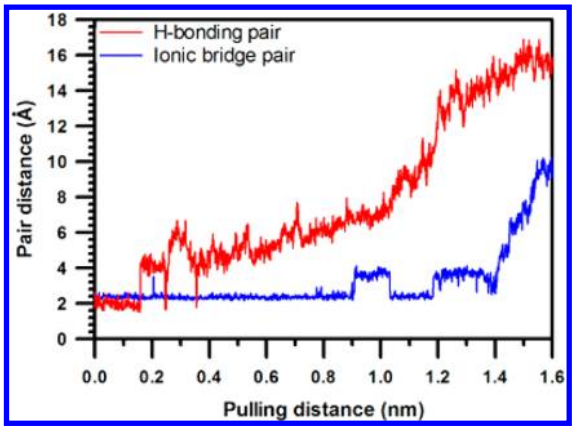

Figure 12. Variations of the atomic pair distances involved in the H-bonding (red) or the ionic bridge binding (blue) versus the pulling distance. The H-bonding pair distance refers to the distance between the oxygen of carboxylate group in PA and the hydrogen of hydroxyl group in alginate. The ionic bridging pair distance refers to the distance between the carboxylate oxygen in alginate and the Ca^{2+} ion involved in binding.

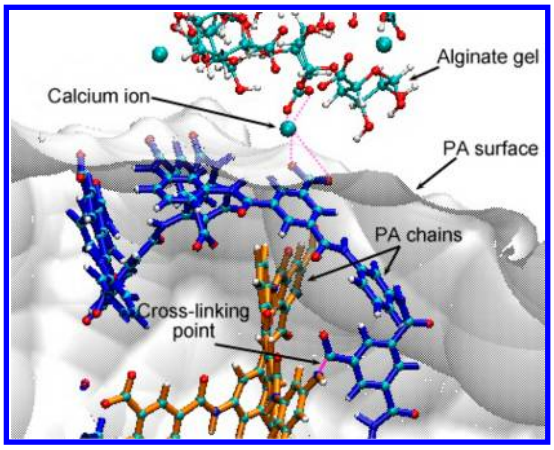

Figure 13. Snapshot of the ionic bridge near the cross-linking point prior to the final breakdown. The last ionic force peak has been shifted to a shorter pulling distance at 1.25 nm (see Figure 10) due the rigidity of the cross-linked PA chain. The ionic bridges are indicated by the purple lines. The two PA chains involved in the ionic bridging are distinguished by different colors.

rate usually results in higher near-surface rigidity and lower survival pulling distances for ionic bridge binding.

4. SUMMARY

In this study, we performed molecular dynamics simulations to investigate the aggregation of multiple alginate molecules, the structure of alginate gel and its interaction with a PA membrane surface. A cross-linked PA membrane in water has been built using a previously established protocol.[18,19] The effect of different metal ions on the formation of alginate gels has been carefully studied. Simulation results show that Ca^{2+} ion has a strong effect on the aggregation of alginate chains to form a gel, mostly through the two-bidentate, inner-sphere binding complexes. The SMD simulation on the alginate gel−PA surface interaction reveal that the adhesion force between the gel and membrane has multiple origins: the hydrogen bonding and van der Waals interaction in the short range, and the ionic bridge binding in the long range due to the chain deformation. The survival pulling distances of ionic bridges are also determined by the rigidity of membrane surface chains. The present study provides valuable information on the fouling mechanism of PA membranes by alginate gel, and the new findings may help to understand the general fouling mechanism by other organic foulants. Therefore, the fundamental insights learned from this work may shed light on other sophisticated membrane fouling problems and may change the way of our thinking about the membrane design in this community.

AUTHOR INFORMATION

Corresponding Author

*Tel 202-994-5964. E-mail leng@gwu.edu.

Notes

The authors declare no competing financial interest.

ACKNOWLEDGMENTS

This work is supported by the National Science Foundation (NSF 1034158) and the National Energy Research Scientific Computing Center (NERSC).

REFERENCES

(1) Elimelech, M. The global challenge for adequate and safe water. *J. Water Supply: Res. Technol.—Aqua* **2006**, *55*, 3−10.
(2) Shannon, M. A.; Bohn, P. W.; Elimelech, M.; Georgiadis, J. G.; Marinas, B. J.; Mayes, A. M. Science and technology for water purification in the coming decades. *Nature* **2008**, *452*, 301−310.
(3) Malaeb, L.; Ayoub, G. M. Reverse osmosis technology for water treatment: State of the art review. *Desalination* **2011**, *267*, 1−8.
(4) Greenlee, L. F.; Lawler, D. F.; Freeman, B. D.; Marrot, B.; Moulin, P. Reverse osmosis desalination: Water sources, technology, and today's challenges. *Water Res.* **2009**, *43*, 2317−2348.
(5) Fritzmann, C.; Lowenberg, J.; Wintgens, T.; Melin, T. State-of-the-art of reverse osmosis desalination. *Desalination* **2007**, *216*, 1−76.
(6) Le-Clech, P.; Chen, V.; Fane, T. A. G. Fouling in membrane bioreactors used in wastewater treatment. *J. Membr. Sci.* **2006**, *284*, 17−53.
(7) Hong, S. K.; Elimelech, M. Chemical and physical aspects of natural organic matter (NOM) fouling of nanofiltration membranes. *J. Membr. Sci.* **1997**, *132*, 159−181.
(8) Iskrenova-Tchoukova, E.; Kalinichev, A. G.; Kirkpatrick, R. J. Metal cation complexation with natural organic matter in aqueous solutions: Molecular dynamics simulations and potentials of mean force. *Langmuir* **2010**, *26*, 15909−15919.
(9) Kalinichev, A. G.; Iskrenova-Tchoukova, E.; Ahn, W. Y.; Clark, M. M.; Kirkpatrick, R. J. Effects of Ca^{2+} on supramolecular aggregation of natural organic matter in aqueous solutions: A comparison of molecular modeling approaches. *Geoderma* **2011**, *169*, 27−32.
(10) Plazinski, W. Molecular basis of calcium binding by polyguluronate chains. Revising the egg-box model. *J. Comput. Chem.* **2011**, *32*, 2988−2995.
(11) Kunhi Mouvenchery, Y.; Kucerik, J.; Diehl, D.; Schaumann, G. E. Cation-mediated cross-linking in natural organic matter: A review. *Rev. Environ. Sci. Bio/Technol.* **2012**, *11*, 41−54.
(12) Plazinski, W.; Rudzinski, W. Molecular modeling of Ca^{2+}-oligo(alpha-l-guluronate) complexes: Toward the understanding of the junction zone structure in calcium alginate gels. *Struct. Chem.* **2012**, *23*, 1409−1415.
(13) Ahn, W. Y.; Kalinichev, A. G.; Clark, M. M. Effects of background cations on the fouling of polyethersulfone membranes by natural organic matter: Experimental and molecular modeling study. *J. Membr. Sci.* **2008**, *309*, 128−140.
(14) Xiang, Y.; Liu, Y. L.; Mi, B. X.; Leng, Y. S. Hydrated polyamide membrane and its interaction with alginate: A molecular dynamics study. *Langmuir* **2013**, *29*, 11600−11608.

(15) Eslami, H.; Muller-Plathe, F. Molecular dynamics simulation of water influence on local structure of nanoconfined polyamide-6,6. *J. Phys. Chem. B* **2011**, *115*, 9720−9731.
(16) Harder, E.; Walters, D. E.; Bodnar, Y. D.; Faibish, R. S.; Roux, B. Molecular dynamics study of a polymeric reverse osmosis membrane. *J. Phys. Chem. B* **2009**, *113*, 10177−10182.
(17) Hughes, Z. E.; Gale, J. D. A computational investigation of the properties of a reverse osmosis membrane. *J. Mater. Chem.* **2010**, *20*, 7788−7799.
(18) Kotelyanskii, M.; Wagner, N. J.; Paulaitis, M. E. Building large amorphous polymer structures: Atomistic simulation of glassy polystyrene. *Macromolecules* **1996**, *29*, 8497−8506.
(19) Kotelyanskii, M. J.; Wagner, N. J.; Paulaitis, M. E. Atomistic simulation of water and salt transport in the reverse osmosis membrane FT-30. *J. Membr. Sci.* **1998**, *139*, 1−16.
(20) Nadler, R.; Srebnik, S. Molecular simulation of polyamide synthesis by interfacial polymerization. *J. Membr. Sci.* **2008**, *315*, 100−105.
(21) Ridgway, H. F.; Gale, J. D.; Hughes, Z. E.; Stewart, M. B.; Orbell, J. D.; Gray, S. R. *Functional nanostructured materials and membranes for water treatment*; Book News, Inc.: Portland, 2013; Vol. *28*.
(22) Lee, S.; Elimelech, M. Relating organic fouling of reverse osmosis membranes to intermolecular adhesion forces. *Environ. Sci. Technol.* **2006**, *40*, 980−987.
(23) Mi, B.; Elimelech, M. Chemical and physical aspects of organic fouling of forward osmosis membranes. *J. Membr. Sci.* **2008**, *320*, 292−302.
(24) Li, Q. L.; Xu, Z. H.; Pinnau, I. Fouling of reverse osmosis membranes by biopolymers in wastewater secondary effluent: Role of membrane surface properties and initial permeate flux. *J. Membr. Sci.* **2007**, *290*, 173−181.
(25) Siepmann, J. I. A method for the direct calculation of chemical potentials for dense chain systems. *Mol. Phys.* **1990**, *70*, 1145−1158.
(26) Frenkel, D.; Smit, B. *Understanding molecular simulation from algorithms to application*. Academic Press: San Diego, 1996.
(27) Ding, M. X.; Szymczyk, A.; Goujon, F.; Soldera, A.; Ghoufi, A. Structure and dynamics of water confined in a polyamide reverse-osmosis membrane: A molecular-simulation study. *J. Membr. Sci.* **2014**, *458*, 236−244.
(28) Tang, C. Y. Y.; Kwon, Y. N.; Leckie, J. O. Effect of membrane chemistry and coating layer on physiochemical properties of thin film composite polyamide RO and NF membranes I. FTIR and XPS characterization of polyamide and coating layer chemistry. *Desalination* **2009**, *242*, 149−167.
(29) Coronell, O.; Marinas, B. J.; Cahill, D. G. Depth heterogeneity of fully aromatic polyamide active layers in reverse osmosis and nanofiltration membranes. *Environ. Sci. Technol.* **2011**, *45*, 4513−4520.
(30) Do, V. T.; Tang, C. Y. Y.; Reinhard, M.; Leckie, J. O. Degradation of polyamide nanofiltration and reverse osmosis membranes by hypochlorite. *Environ. Sci. Technol.* **2012**, *46*, 852−859.
(31) Mi, B. X.; Coronell, O.; Marinas, B. J.; Watanabe, F.; Cahill, D. G.; Petrov, I. Physico-chemical characterization of NF/RO membrane active layers by Rutherford backscattering spectrometry. *J. Membr. Sci.* **2006**, *282*, 71−81.
(32) Leng, Y. S. Hydration force between mica surfaces in aqueous KCl electrolyte solution. *Langmuir* **2012**, *28*, 5339−5349.
(33) Leng, Y. S. Hydration force and dynamic squeeze-out of hydration water under subnanometer confinement. *J. Phys.: Condens. Matter* **2008**, *20*, 354017−354024.
(34) Perry, T. D.; Cygan, R. T.; Mitchell, R. Molecular models of alginic acid: Interactions with calcium ions and calcite surfaces. *Geochim. Cosmochim. Acta* **2006**, *70*, 3508−3532.
(35) Davis, T. A.; Volesky, B.; Mucci, A. A review of the biochemistry of heavy metal biosorption by brown algae. *Water Res.* **2003**, *37*, 4311−4330.
(36) Brown, T.; LeMay, E. H.; Bursten, B.; Murphy, C.; Woodward, P. *Chemistry: The Central Science*; Prentice Hall: Boston, 2011.
(37) Plimpton, S. Fast parallel algorithms for short range molecular dynamics. *J. Comput. Phys.* **1995**, *117*, 1−19.
(38) Kitson, D. H.; Hagler, A. T. Theoretical studies of the structure and molecular dynamics of a peptide crystal. *Biochemistry* **1988**, *27*, 5246−5257.
(39) Berendsen, H. J. C.; Postma, J. P. M.; van Gunsteren, W. F.; Hermans, J. *Interaction models for water in relation to protein hydration*; D. Riedel Publishing Co.: Dordrecht, The Netherlands, 1981.
(40) Teleman, O.; Jonsson, B.; Engstrom, S. A molecular dynamics simulation of a water model with intramolecular degrees of freedom. *Mol. Phys.* **1987**, *60*, 193−203.
(41) Aqvist, J. Ion water interaction potentials derived from free-energy perturbation simulations. *J. Phys. Chem.* **1990**, *94*, 8021−8024.
(42) Joung, I. S.; Cheatham, T. E. Determination of alkali and halide monovalent ion parameters for use in explicitly solvated biomolecular simulations. *J. Phys. Chem. B* **2008**, *112*, 9020−9041.
(43) Hockney, R. W.; Eastwood, J. W. *Computer Simulation Using Particles*; Taylor and Francis Group: London, 1988.
(44) Braccini, I.; Grasso, R. P.; Perez, S. Conformational and configurational features of acidic polysaccharides and their interactions with calcium ions: a molecular modeling investigation. *Carbohydr. Res.* **1999**, *317*, 119−130.
(45) Peric, L.; Pereira, C. S.; Perez, S.; Hunenberger, P. H. Conformation, dynamics and ion-binding properties of single-chain polyuronates: a molecular dynamics study. *Mol. Simul.* **2008**, *34*, 421−446.
(46) Seale, R.; Morris, E. R.; Rees, D. A. Interactions of alginates with univalent cations. *Carbohydr. Res.* **1982**, *110*, 101−112.
(47) Braccini, I.; Perez, S. Molecular basis of Ca^{2+}-induced gelation in alginates and pectins: The egg-box model revisited. *Biomacromolecules* **2001**, *2*, 1089−1096.
(48) Peric-Hassler, L.; Hunenberger, P. H. Interaction of alginate single-chain polyguluronate segments with mono- and divalent metal cations: A comparative molecular dynamics study. *Mol. Simul.* **2010**, *36*, 778−795.
(49) Sutton, R.; Sposito, G.; Diallo, M. S.; Schulten, H. R. Molecular simulation of a model of dissolved organic matter. *Environ. Toxicol. Chem.* **2005**, *24*, 1902−1911.
(50) Pavlov, M.; Siegbahn, P. E. M.; Sandstrom, M. Hydration of beryllium, magnesium, calcium, and zinc ions using density functional theory. *J. Phys. Chem. A* **1998**, *102*, 219−228.
(51) Jensen, K. P.; Jorgensen, W. L. Halide, ammonium, and alkali metal ion parameters for modeling aqueous solutions. *J. Chem. Theory Comput.* **2006**, *2*, 1499−1509.
(52) Baker, R. W. *Membrane technology and applications*; McGraw-Hill: New York, 2000.
(53) Luzar, A.; Chandler, D. Effect of environment on hydrogen bond dynamics in liquid water. *Phys. Rev. Lett.* **1996**, *76*, 928−931.
(54) Lei, Y. J.; Leng, Y. S. Hydrophobic drying and hysteresis at different length scales by molecular dynamics simulations. *Langmuir* **2012**, *28*, 3152.
(55) Zhou, R. H.; Huang, X. H.; Margulis, C. J.; Berne, B. J. Hydrophobic collapse in multidomain protein folding. *Science* **2004**, *305*, 1605−1609.